

pubs.acs.org/acsaelm Article

Role of Heterointerface in Lithium-Induced Phase Transition in T_d-WTe₂ Nanoflakes

Shiyu Xu, Mengjing Wang, Maria Bambrick-Santoyo, Kenneth Evans-Lutterodt, Natalie L. Williams, and Judy J. Cha*



Cite This: ACS Appl. Electron. Mater. 2024, 6, 785–792



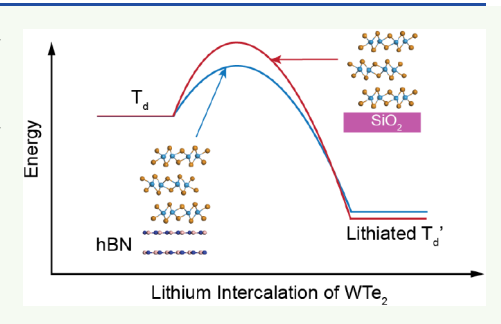
ACCESS I

Metrics & More

Article Recommendations

Supporting Information

ABSTRACT: A new polytype of WTe2 with a bandgap has been recently discovered through the intercalation of lithium into the van der Waals gaps of T_d-WTe2. Here, we report the effects of reduced thicknesses and heterointerfaces on the intercalation-induced phase transition in WTe2. Using in situ Raman spectroscopy during the electrochemical lithiation of WTe2 flakes as a function of flake thickness, we observe that additional electrochemical energy is required for the phase transition of WTe₂ from the T_d phase to the new lithiated T_d phase, going from 0.8 V of the applied electrochemical voltage for a thick flake to 0.5 V and 0.3 V for 7- and 5layered samples, respectively. We ascribe this suppression of the phase transition to the interfacial interaction between the nanoflake and SiO₂/Si substrate, which plays an increasing role as the sample thickness is reduced. The suppressed kinetics of the



phase transition can be mitigated by placing the WTe₂ flake on a hexagonal boron nitride (hBN) flake, which facilitates the release of the in-plane strain induced by the phase transition. Our study underscores the significance of interfacial effects in modulating phase transitions in two-dimensional (2D) materials, suggesting heterogeneous transition pathways, as well as interfacial engineering to control these phase transitions.

KEYWORDS: lithium intercalation, phase transition, interface, WTe2-hBN interface, in situ Raman spectroscopy

INTRODUCTION

Two-dimensional (2D) transition metal dichalcogenides (TMDCs) have been extensively studied for their potential in various cutting-edge applications such as optoelectronics, electronics, catalysis, and energy storage, owing to their numerous structural polymorphs. 1-6 Phase transitions in 2D TMDCs can be realized through methods including charge doping,⁷ strain engineering,⁸ intercalation,^{9,10} thermal treatment,¹¹ and light irradiation.¹² Phase transitions in monolayer or few-layered TMDCs are highly desirable to minimize power consumption and realize ultimate scalability in many applications. 13,14 However, reduced thicknesses and the presence of heterointerfaces can significantly alter the phase transition thermodynamics and kinetics, 15-18 requiring a detailed understanding of the effects of thickness confinement and heterointerfaces for successful applications of 2D materials. Among 2D TMDCs, orthorhombic tungsten ditelluride (T_d-WTe₂) stands out as a type-II Weyl semimetal in bulk, and a topological insulating phase, 19 superconductivity, 20-22 and ferroelectricity 23 have been observed in the monolayer limit. A new polytype of T_d-WTe₂, driven by lithiation, was recently discovered, exhibiting a unique crystal structure $(T_d')^{24}$ with a bandgap opening of 0.14 eV.²⁵ This discovery makes T_d-WTe₂ promising for applications in strained actuators and resistive memory. Yet, this phase transition was observed only in T_d-WTe₂ nanoflakes thicker

than 30 nm, and effects of reduced thickness and heterointerface have not been explored.

In this study, we investigate the impact of thicknesses and heterointerfaces on the phase transition of WTe₂ from the semimetallic T_d phase to the new lithiated T_d phase. This transformation was achieved by electrochemically inserting lithium into the van der Waals (vdW) gaps of the T_d-WTe₂ flake. For T_d-WTe₂ flakes with thicknesses raging from 30 to 100 nm (>40 layers), the phase transition occurred at an applied electrochemical intercalation voltage of 0.8 V, as evident from the emergence of a distinct Raman spectrum and a lattice expansion in the out-of-plane direction. By contrast, for 7- and 5-layered T_d -WTe₂ flakes, the electrochemical intercalation voltage required for the phase transition was lowered to 0.5 V, indicating a change of phase transition energetics and a suppressed phase transition. We attribute this suppression to the strong interfacial interaction between the T_d-WTe₂ flake and the SiO₂/Si substrate. This interfacial effect becomes more pronounced for thinner flakes and hinders the

Received: September 21, 2023 Revised: January 22, 2024 Accepted: January 24, 2024 Published: February 14, 2024





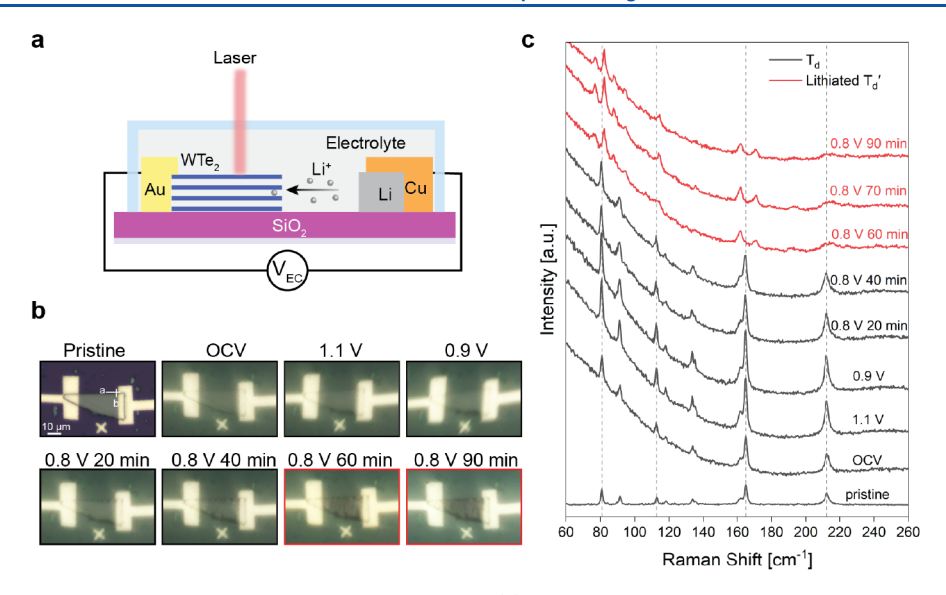


Figure 1. Lithium-induced phase transition in a thick T_d -WTe₂ nanoflake. (a) Schematic of a planar electrochemical intercalation cell with *in situ* Raman capability. $V_{\rm EC}$ stands for the electrochemical intercalation voltage applied between the single crystalline T_d -WTe₂ nanoflake and the lithium electrode. (b) Optical images of a thick T_d -WTe₂ nanoflake as a function of $V_{\rm EC}$ using a polymer electrolyte; scale bar 10 μ m. The black and red frames represent the T_d and lithiated T_d phases, respectively. The T_d to T_d phase transition is accompanied by the emergence of optically dark streaks across the nanoflake. (c) *In situ* Raman spectra of the T_d -WTe₂ nanoflake in (b) as a function of intercalation voltage. The black and red spectra represent the T_d and lithiated T_d phases, respectively.

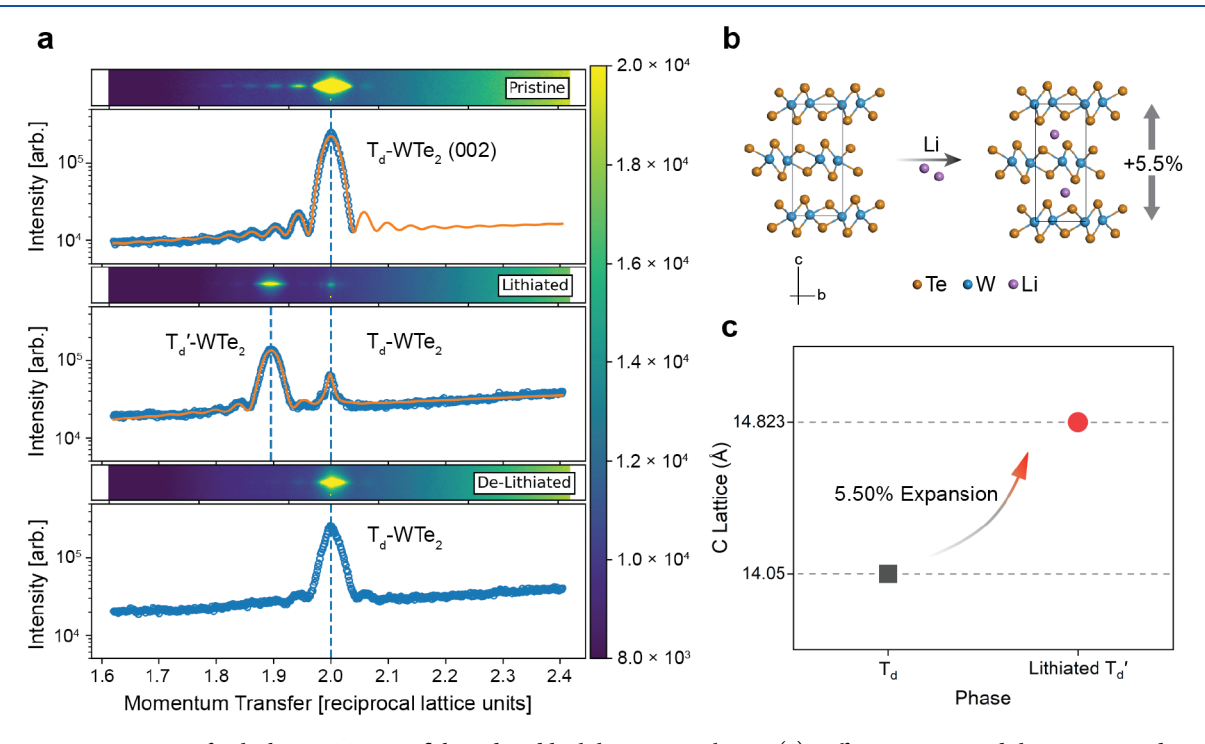


Figure 2. Lattice expansion of a thick T_d -WTe₂ nanoflake induced by lithium intercalation. (a) Diffraction spots and their corresponding intensity profiles of the (002) plane in the reciprocal space by single-crystal XRD collected from a thick T_d -WTe₂ nanoflake at the pristine T_d (top), lithiated T_d (middle), and delithiated T_d (bottom) phases, respectively. (b) Side view of the structure change in the c direction of T_d -WTe₂ induced by lithium intercalation. Te: gold, W: blue, Li: purple. (c) Lattice expansion in the c direction between the T_d and lithiated T_d phases derived from single-crystal XRD.

release of the in-plane strain introduced during the phase transition. Heterointerface engineering, whereby a WTe $_2$ -hBN interface was introduced to help facilitate the in-plane strain release, can mitigate the phase transition delay for thin WTe $_2$ flakes. Our observations underscore the significant influence of thickness and substrate heterointerfaces on phase transition dynamics of 2D materials.

RESULTS AND DISCUSSION

Electrochemical Intercalation in Thick $T_{\rm d}$ -WTe₂ Nano-flakes. Electrochemical intercalation cells that incorporate nanodevices were used to understand the phase transition of $T_{\rm d}$ -WTe₂ flakes induced by lithium intercalation. These cells enable *in situ* Raman spectroscopy or single-crystal X-ray diffraction (XRD) measurements as a function of intercalation

ACS Applied Electronic Materials

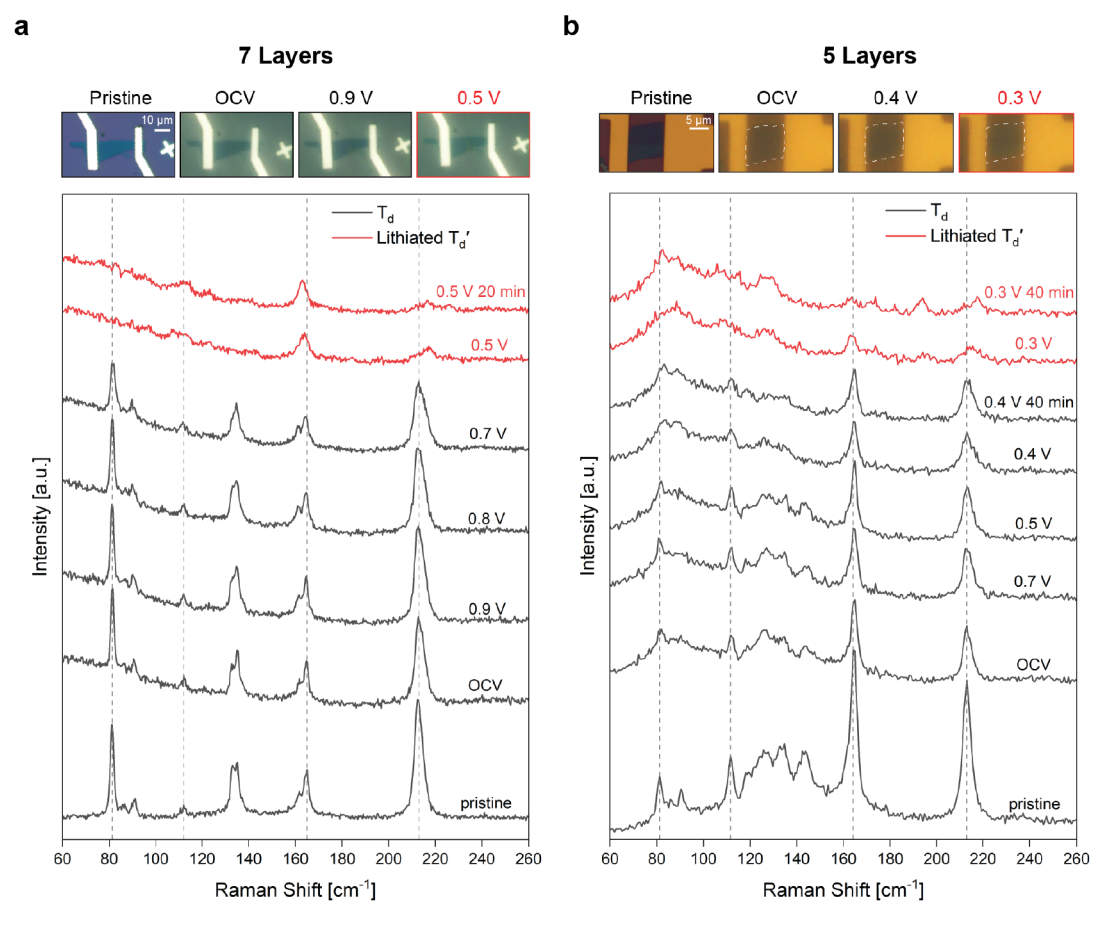


Figure 3. Delayed $T_{\rm d}$ to lithiated $T_{\rm d}'$ phase transition observed in few-layered samples. (a, b) Optical images (top) and in situ Raman spectra (bottom) of a 7-layered (a) and a 5-layered (b) $T_{\rm d}$ -WTe₂ nanoflake during lithium intercalation; scale bar, 10 μ m in (a) and 5 μ m in (b). Black and red spectra represent the $T_{\rm d}$ and lithiated $T_{\rm d}'$ phases, respectively.

(Figure 1a, Experimental Methods). The mechanically exfoliated $T_{\rm d}$ -WTe $_2$ flakes were 20–50 μ m in lateral dimensions and 30–100 nm (>40 layers) in thickness. Both liquid and polymer-based electrolytes were used for lithium intercalation (details in Experimental Methods). By applying a controlled electrochemical intercalation voltage ($V_{\rm EC}$) between the single crystalline $T_{\rm d}$ -WTe $_2$ flake (cathode) and the lithium (Li, anode), lithium ions (Li⁺) are controllably driven and inserted into the vdW gaps of the $T_{\rm d}$ -WTe $_2$ flake. The applied $V_{\rm EC}$ lies between the open-circuit voltage (OCV, typically 2.3–2.8 V vs Li⁺/Li) and 0.1 V (vs Li⁺/Li). A lower V_{EC} corresponds to higher lithium concentrations in the $T_{\rm d}$ -WTe $_2$ flake, allowing for fine-tuning of the intercalation concentrations.

As reported previously by Muscher et al. 24 and Wang et al., 25 we observe a new polytype in WTe₂ flakes by intercalating lithium, which was confirmed by distinct Raman peaks that emerge at $V_{\rm EC}$ of 0.8 V vs Li⁺/Li for a polymer cell (Figure 1c) and of 1.2 V vs Li⁺/Li for a liquid cell (Figure S1). Raman peaks corresponding to $T_{\rm d}$ -WTe₂ at \sim 80.8, \sim 113, \sim 134, \sim 165, and \sim 212 cm⁻¹ (Table S1) displayed noticeable shifts, broadening, or weakening, while several small new peaks emerged. The Raman spectrum of this new phase is that of lithiated $T_{\rm d}$ -WTe₂. Optical images showed dark streaks in the lithiated $T_{\rm d}$ -WTe₂ along crystallographic axis b, which is perpendicular to the W–W chain of pristine $T_{\rm d}$ -WTe₂ (Figure 1b). These streaks were identified as wrinkles in the flake, as confirmed by scanning electron microscopy (SEM) on a

postintercalation cell (Figure S1). The formation of wrinkles is a result of the anisotropic in-plane strain introduced during the $T_{\rm d}$ to $T_{\rm d}{}'$ phase transition.

Lattice Expansion of Lithiated T_{d} -WTe₂ Nanoflakes. In addition to the in-plane strain, an out-of-plane expansion was observed through the change in the reciprocal lattice of the (002) plane, as determined by in situ single-crystal XRD during electrochemical lithiation on individual flakes. Figure 2a illustrates the reciprocal lattice of the (002) plane for pristine T_{d} -WTe₂ (top), lithiated T_{d} -WTe₂ (middle), and delithiated T_{d} -WTe₂ (bottom). In comparison to pristine T_{d} -WTe₂, lithiated T_d -WTe₂ shows a smaller lattice of the (002) plane in reciprocal space, which corresponds to an expansion in the out-of-plane c direction in real space. The c lattice of lithiated T_d'-WTe₂ was measured to be 14.82 Å, while that of the pristine T_d -WTe₂ was 14.05 Å (Figure 2c), representing a \sim 5.5% expansion of c lattice (Figure 2b). As studied by Whittingham et al., this lattice expansion is due to the repulsive forces between lithium ions and chalcogenide layers.²⁹ Notably, the copresence of the intense peak of lithiated T_d '-WTe2 and the weaker peak of Td-WTe2 indicates an incomplete phase transition of the T_d-WTe₂ nanoflake, which is a common occurrence in thick flakes. The ratio of the integrated intensity of the lithiated T_d -WTe₂ peak to the T_d -WTe₂ peak is 10.2 ± 0.2 . After the acquisition of single-crystal XRD for the lithiated $T_{\rm d}$ '-WTe₂, the applied $V_{\rm EC}$ was removed, allowing for the nanoflake to recover to its original T_d phase. This recovery was confirmed by the disappearance of the

lithiated $T_{\rm d}$ -WTe₂ peak and restoration of a high intensity of the $T_{\rm d}$ -WTe₂ peak. This result demonstrates the reversibility of the $T_{\rm d}$ and $T_{\rm d}$ ' phase transition.

Delayed Phase Transition in Few-layered T_d-WTe₂ Nanoflakes. Next, we performed lithium intercalation in the thinner T_d-WTe₂ nanoflakes. While thicker T_d-WTe₂ flakes underwent the phase transition from $T_{\rm d}$ to the lithiated $T_{\rm d}$ phase at an applied $V_{\rm EC}$ of 0.8 V (vs Li⁺/Li), the same phase transition did not occur until 0.5 V (vs Li+/Li) for a 7-layered T_d-WTe₂ flake, as shown in Figure 3a. Optical images showed no obvious dark streaks after the T_d to T_d phase transition; but small wrinkles were observed with SEM postintercalation (Figure S2). For a 5-layered T_d -WTe₂ flake, in situ Raman peaks persisted even at 0.4 V for over 40 min before eventually changing at 0.3 V (Figure 3b). Thus, our key finding is that thin $T_{\mathrm{d}}\text{-WTe}_2$ flakes require more applied V_{EC} to induce the phase transition from $T_{\rm d}$ to the lithiated $T_{\rm d}{}'$ phase, indicating a suppression of the phase transition. Thinner flakes tend to be smaller in their lateral dimensions. Thus, we also examined whether the lateral size of the flake would impact the phase change significantly. We verify that the thickness effect is much more significant than the effect of the flake size (Figure S3).

We consider several possibilities that can explain the suppression of the phase transition for thinner flakes: thickness-dependent band structure of T_d-WTe₂, suppressed nucleation of a $T_{\rm d}$ phase with decreasing thickness, thicknessdependent bending-induced strain introduced by the out-ofplane expansion, and substrate interactions. These possibilities are discussed in order. First, if the band structure of T_d -WTe₂ changes with thickness, this might influence the intercalationinduced phase change as the process of lithium intercalation is to align the Fermi level between lithium and WTe2. We rule this out because the semimetallic nature of T_d -WTe₂ remains mostly unchanged with decreasing thickness.³⁰ The second possibility involves the suppression of nucleation of the new phase in thin flakes based on our classical understanding of a critical nucleus size. This is unlikely based on our previous studies, which suggest that the intercalation-induced phase change is initiated at the topmost or bottom most layer, 16 and these phase transitions occur in a layer-by-layer fashion in 2D materials; $^{31-33}$ thus nucleation of the $T_{\rm d}{}'$ phase should be insensitive to flake thickness. The third possibility to explain the suppressed phase transition is bending induced in-plane strain due to the c-axis lattice expansion, which might introduce an additional energy barrier to the phase transition. This is what we previously observed in delayed lithium staging in thick graphite flakes.³⁴ For the phase transition in WTe₂, we observe a c-axis lattice expansion of more than 5% (Figure 2). However, we do not observe any shifts of Raman peaks in T_{d} -WTe₂ during intercalation (Figure S4), which would indicate in-plane tensile strain.³⁵ Interpreting peak shifts in Raman spectra for WTe2 is complicated by the fact that electron doping and tensile strain, both of which lithium intercalation imparts to WTe2, would result in the opposite shifts in Raman peaks.³⁶ Nevertheless, the bending-induced strain is unlikely the cause for our observation, because the bending-induced strain would increase with increasing thickness, further delaying the phase transition for thicker flakes, which we do not observe.

Finally, we turn our attention to the interface interaction between the SiO_2/Si substrate and the T_d -WTe₂ flake during the phase transition. Compared to the T_d -WTe₂ phase, lithiated T_d -WTe₂ exhibits an in-plane lattice expansion of

5.2% and 0.2% along the a- and b-axes, respectively, which is concurrent with the rearrangement of tellurium atoms.²⁴ The significant expansion of the structure induces in-plane strain, which leads to the formation of wrinkled microstructures in WTe₂ flakes supported on the SiO₂/Si substrate (Figures S1 and S2). This in-plane strain is distinct from the bendinginduced strain due to the lattice expansion along the c-axis discussed previously. Our hypothesis is that the interface between the T_d -WTe₂ flake and the SiO₂/Si substrate anchors the nanoflake, preventing the release of the in-plane strain introduced during the $T_{\rm d}$ to $T_{\rm d}{}^{\prime}$ phase transition, thus increasing the energy barrier of the phase change. The interfacial effect is likely to affect the bottommost layer of the T_d -WTe₂ flake that directly contacts the SiO₂/Si substrate. In this case, the substrate effect becomes more pronounced in atomically thin layered samples compared to thicker samples.

Effects of Substrate Interfaces on Phase Transition Kinetics. To test our hypothesis of the interface effect due to the interaction between the substrate and WTe₂, we place our WTe₂ flakes on hBN to weaken the interactions at this heterointerface. An atomic force microscopy (AFM) study has shown that coupling between SiO₂ and Bi₂Se₃ layer is stronger than that between Bi₂Se₃ layers,³⁷ supporting our rationale of using hBN. Figure 4 shows a thick T_d -WTe₂ flake (>100 nm) that was partially placed on the top of a hBN flake and partially

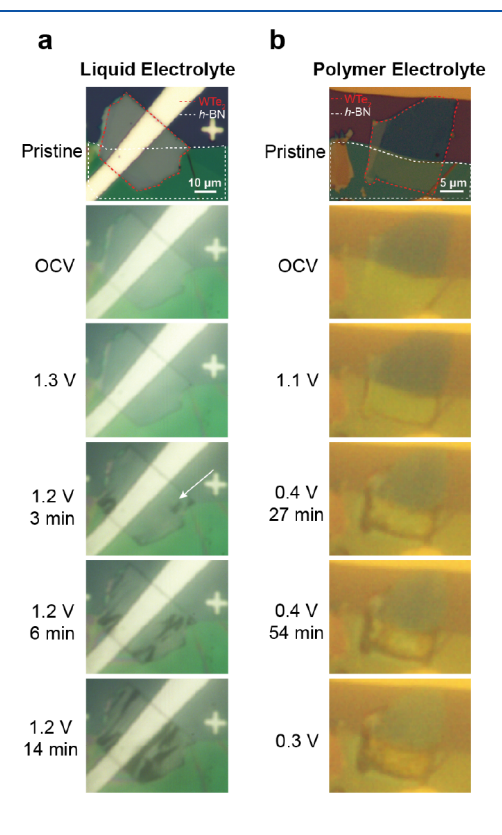


Figure 4. Comparison of phase transition kinetics in $T_{\rm d}$ -WTe $_2$ with different substrate interfaces. (a) Optical images of a $T_{\rm d}$ -WTe $_2$ nanoflake (red dashed outline) partially supported on an hBN flake (white dashed outline) during lithium intercalation using liquid electrolyte; scale bar, 10 μ m. The appearance of dark streaks marks the onset of the phase transition from $T_{\rm d}$ to lithiated $T_{\rm d}$ '. (b) Optical images of a $T_{\rm d}$ -WTe $_2$ nanoflake (red dashed outline) partially supported on a hBN flake (white dashed outline) collected during lithium intercalation using a polymer electrolyte; scale bar: 5 μ m. The Raman spectra for (b) are shown in Figure S5.

on the SiO $_2$ /Si substrate. This heterostructure was then assembled into a liquid intercalation cell with the Cr/Au electrode contacting both $T_{\rm d}$ -WTe $_2$ and hBN. At an $V_{\rm EC}$ of 1.2 V, dark streaks that represent wrinkles appeared, thus signifying the phase transition, which first appeared along the edge of the hBN-supported region after 3 min, then for the entire hBN-supported region after 6 min (Figure 4a). By contrast, it took 14 min for the wrinkles to appear in the solely SiO $_2$ /Si supported region. This observation supports the hypothesis that the weak interfacial coupling between $T_{\rm d}$ -WTe $_2$ and hBN facilitated the release of in-plain strain introduced by the $T_{\rm d}$ to $T_{\rm d}$ ' phase transition during lithium intercalation, unlike the interface between $T_{\rm d}$ -WTe $_2$ and the SiO $_2$ /Si substrate.

The rapid phase transition due to the high ionic conductivity of the liquid electrolyte made it challenging to acquire Raman spectra during intercalation. Therefore, we fabricated a polymer cell featuring a 5-layered T_d-WTe₂ flake, half supported on a hBN flake and the other half directly on the SiO₂/Si substrate (Figure 4b). Raman spectra collected during lithium intercalation of this cell are presented in Figure S5, which shows that the T_d to T_d phase transition occurred at 0.3 V for the SiO_2 -supported T_d -WTe₂ region, which is consistent with the suppressed phase transition discussed earlier. For the hBN supported T_d-WTe₂ region, the Raman spectra changed at 0.4 V, confirming our hypothesis that anchoring to the SiO₂/Si substrate results in the delay of the phase transition in thin T_d-WTe₂ nanoflakes. We note that additional substrate effects may be at play, such as surface roughness of the SiO₂ layer that may impact lithium intercalation, 38 inhomogeneous charge transfer from the SiO₂ substrate to the T_d-WTe₂ flake due to defects associated with amorphous SiO2 in contrast to hBN, 39,40 and lattice mismatch between WTe2 and the underlying substrate.

CONCLUSION

In summary, our study shows that the $T_{\rm d}$ to lithiated $T_{\rm d}'$ phase transition of WTe₂ flakes is thickness dependent with more applied electrochemical voltages needed for thinner flakes, going from an intercalation voltage of 0.8 V for thicker flakes to 0.5 V for a 7-layered flake and to 0.3 V for a 5-layered flake to trigger the phase transition using a polymer electrolyte. Table 1

Table 1. Summary of Measured $T_{\rm d}$ -WTe₂ Flakes with Their Number of Layers, Substrate, and Voltage Needed for the Phase Transition from the $T_{\rm d}$ to $T_{\rm d}$ 'Phase

sample #	number of layers	substrate	voltage of the phase transition (V, vs $\text{Li}^{\text{+}}/\text{Li}$)
1	>40	SiO ₂ /Si	0.8
2	7	SiO ₂ /Si	0.5
3	5	SiO ₂ /Si	0.3
4 ^a	5	SiO ₂ /Si	0.3
		hBN	0.4

^aA 5-layered T_{d} -WTe₂ flake that is half directly on the SiO₂/Si substrate and the other half supported on a hBN flake.

summarizes our main findings. We attribute our observation to strong interactions between WTe_2 and the SiO_2/Si substrate, which hinder the effective release of the in-plane strain in WTe_2 during the phase transition. This interfacial interaction becomes more prominent as the thickness of the flake decreases. The observed suppression of the phase transition

can be mitigated by proper interface engineering, such as replacing the SiO_2/Si substrate with an hBN flake. Our observations highlight the unique interface interactions of WTe₂, particularly in thinner nanoflakes, during the lithium intercalation process. Such heterointerface effects hold implications for various device applications reliant on phase changes, as they can alter the phase transition dynamics.

EXPERIMENTAL METHODS

Device Fabrication. T_d-WTe₂ and hBN nanoflakes were obtained via mechanical exfoliation from WTe_2 (2D semiconductors) and hBN (HQ graphene) bulk by scotch-tape onto SiO₂/Si substrates. Subsequently, a potassium hydroxide (KOH)-assisted transfer method was employed to transfer desired size- and thicknesscontrolled T_d-WTe₂ nanoflakes onto dry thermal oxide SiO₂/Si substrates (300 nm SiO₂) with alignment marks for lithography. 15 fabricate the T_d-WTe₂ (top)-hBN (bottom) device, a hBN nanoflake was initially transferred by the same method and then stacked with a WTe2 nanoflake that sat partially on the hBN nanoflake and partially on the dry thermal oxide SiO_2/Si substrate. The thickness of the T_{d} WTe₂ nanoflakes, ranging from 15 layers to bulk, was determined by a Cypher ES atomic force microscope (AFM) from Asylum Research and a Veeco Dimension Icon AFM. ARROW-NCR AFM probes from NanoWorld were used in noncontact mode imaging. As thin WTe₂ nanoflakes are more likely to form oxides compared to thick WTe2 nanoflakes, the ascertainment of thickness of WTe2 nanoflakes with 2-15 layers was not conducted by AFM in air; instead, Raman spectroscopy was employed before the intercalation experiment, where thin WTe2 nanoflakes were protected by an airtight case. The thickness calibration for the WTe2 flakes is shown in Figure S6.

Both e-beam lithography and photolithography were used for the device fabrication. For e-beam lithography, electrodes were patterned using Nabity NPGS (installed on a Helios G4 FIB-SEM) and deposited with 10 nm of Cr/100 nm of Au using thermal evaporation (MBraun EcoVap). E-beam lithography was used to fabricate devices of WTe₂ (thick and 7-layer flakes) and WTe₂—hBN heterostructures (using liquid electrolyte), as well as thick $T_{\rm d}$ -WTe₂ flakes for single-crystal XRD experiments. For some devices, electrodes were written using photolithography (Heidelberg Mask Writer, DWL66FS) and deposited with 10 nm Cr/100 nm Au using an e-beam evaporator (CVC SC4500 Combination Thermal/E-gun Evaporation System). Devices of 5-layered $T_{\rm d}$ -WTe₂ and $T_{\rm d}$ -WTe₂—hBN heterostructures for the polymer cell were fabricated this way. All fabricated devices were stored in an argon glovebox to minimize oxidation.

Fabrication of Electrochemical Intercalation Cells. All electrochemical intercalation cells adopted the same planar cell configuration with a T_d-WTe₂ nanoflake or a T_d-WTe₂-hBN heterostructure as the working electrode and a small piece of lithium metal (~3 mm × 3 mm, 0.38 mm-thick ribbon, Sigma-Aldrich) as the counter/reference electrode. The cell fabrication steps are described in detail in our previous papers. ^{15,16} The entire cell was encapsulated in a transparent case with a coverslip serving as the top cover, allowing the laser to interact with the nanoflake during Raman spectroscopy. For liquid intercalation cells, 1 M lithium hexafluorophosphate (LiPF₆ in 50/50 v/v EC/DEC, battery-grade, Sigma-Aldrich) was injected into the transparent case as the electrolyte. For the polymer electrolyte cells, 227 mg of 1 M LiPF₆, 475 mg of poly(ethylene glycol)methyl ether methacrylate (PEGMA, Sigma-Aldrich) and 1145 mg of bisphenol A ethoxylate (15EO/phenol) dimethacrylate (BEMA, Sigma-Aldrich) were premixed for 4 h. Following this, 46 mg of 2-hydroxy-2-methylpropiophenone (photoinitiator, Sigma-Aldrich) was added to the blend and stirred for another half hour in the dark prior to use. The mixed polymer was carefully filled into the transparent case of the intercalation cell by a micropipette and subsequently cured by exposure to ultraviolet light (UV light, 375 nm, 4 W) for 10 min to form a solid polymer electrolyte. All assembly procedures for the electrochemical intercalation cells were conducted inside the argon glovebox with the O₂ and H₂O levels below 0.5 ppm. With the protection provided by the transparent case, the

intercalation cell can withstand exposure to air and moisture in the atmosphere for a minimum of 10 h, making it suitable for subsequent in situ characterization.

In Situ Raman Characterization. Lithium intercalation of the assembled electrochemical intercalation cell was carried out potentiostatically by applying a voltage between the working ($T_{\rm d}$ -WTe₂ or $T_{\rm d}$ -WTe₂-hBN) and counter/reference (Li) electrodes with a Biological SP300 potentiostat/galvanostat. In situ Raman spectra were collected during lithium intercalation, and two types of Raman spectrometers were used. For the cells of $T_{\rm d}$ -WTe₂ (thick and 7-layers) and $T_{\rm d}$ -WTe₂-hBN heterostructure (using liquid electrolyte), a Horiba LabRAM HR Evolution Spectrometer (grating: 1800 lines/mm) with an excitation wavelength of 633 nm at 10% power (~3.5 mW) was used. For the cells of 5-layered $T_{\rm d}$ -WTe₂ and $T_{\rm d}$ -WTe₂-hBN heterostructure in the polymer cell, a WITec Alpha300R Confocal Raman Microscope (grating: 1800 lines/mm) with a laser wavelength of 532 nm and power ranging from 1 to 3 mW was employed.

Prior to intercalation, a Raman spectrum was acquired at the open circuit voltage (OCV), typically ranging between 2.3 and 2.8 V vs Li⁺/Li for $T_{\rm d}$ -WTe₂ intercalation cells. During the electrochemical intercalation, the voltage applied between the $T_{\rm d}$ -WTe₂ nanoflake and the lithium electrode ($V_{\rm EC}$) was lowered at a controlled rate of 10 mV/s and then maintained at the desired voltage until multiple Raman spectra were collected. Simultaneously, optical images were captured using the camera of the Raman microscope, and the contrast of those images was changed to clearly observe the wrinkle formation during intercalation. The observed differences in contrast and brightness between the pristine $T_{\rm d}$ -WTe₂ and other optical images during intercalation are attributed to the presence of the electrolyte and coverslip.

In Situ Single-Crystal XRD Characterization. The single-crystal X-ray diffraction (XRD) experiments were carried out at beamline 4-ID Integrated In Situ and Resonant Hard X-ray Studies (ISR) of National Synchrotron Light Source II at Brookhaven National Laboratory, using a beam energy of 11.5 keV and a spot size of 40 μ m × 300 μ m. The configuration of the electrochemical intercalation cells for the single-crystal XRD differs slightly from that in the Raman spectroscopy study. An ample amount of polymer electrolyte was carefully applied on the device, covering both the T_d -WTe₂ device and Li and then cured by UV light for 10 min without the transparent coverslip. This cured polymer electrolyte provided sufficient protection for the T_d -WTe₂ device and Li against air and moisture for at least 3 h, allowing the intercalation experiments to be completed within 2 h. However, prolonged X-ray exposure gradually deteriorated the polymer electrolyte, leading to disconnection of the intercalation cell circuit. The lithiated T_d phase reverted to the T_d phase immediately after the cell circuit was disconnected. To mitigate this issue, the X-ray beam exposure was kept to a minimum and solely focused on collecting data related to the Bragg reflection change in the reciprocal lattice of the (002) plane.

Postintercalation SEM Characterization. After electrochemical intercalation, the cells were dissembled, and the electrolyte was carefully removed. Then, the $T_{\rm d}$ -WTe₂ devices were washed with isopropyl alcohol, dried, and characterized by a scanning electron microscope (HeliosG4 FIB-SEM or Tescan Mira3 FESEM) at various tilt angles of 0°, 45°, and 50°.

XPS Characterization. X-ray photoelectron spectroscopy (XPS) characterization of $T_{\rm d}$ -WTe₂ flakes was carried out through a Thermo Nexsa G2 XPS Surface Analysis System (Figure S7).

ASSOCIATED CONTENT

Supporting Information

The Supporting Information is available free of charge at https://pubs.acs.org/doi/10.1021/acsaelm.3c01329.

Lithium intercalation of a liquid cell using a thick $T_{\rm d}$ -WTe₂ flake, postintercalation SEM images of a few-layered $T_{\rm d}$ -WTe₂ nanoflake in a polymer cell, voltage of

phase transition $T_{\rm d}$ to $T_{\rm d}'$ -WTe $_2$ as a function of thickness, peak shift of Raman active modes in $T_{\rm d}$ -WTe $_2$ flakes as a function of intercalation voltage before the phase transition, Raman spectra of WTe $_2$ using different substrates during lithium intercalation, thickness-dependent Raman spectroscopy, XPS of $T_{\rm d}$ -WTe $_2$ flakes; comparison of Raman active mode (PDF)

AUTHOR INFORMATION

Corresponding Author

Judy J. Cha — Department of Materials Science and Engineering, Cornell University, Ithaca, New York 14853, United States; © orcid.org/0000-0002-6346-2814; Email: jc476@cornell.edu

Authors

Shiyu Xu — Department of Materials Science and Engineering, Cornell University, Ithaca, New York 14853, United States; Department of Mechanical Engineering and Materials Science, Yale University, New Haven, Connecticut 06511, United States; orcid.org/0000-0002-3061-632X

Mengjing Wang — Department of Materials Science and Engineering, Cornell University, Ithaca, New York 14853, United States

Maria Bambrick-Santoyo — Department of Applied Physics, Yale University, New Haven, Connecticut 06511, United States

Kenneth Evans-Lutterodt — National Synchrotron Light Source II, Brookhaven National Laboratory, Upton, New York 11973, United States

Natalie L. Williams – Department of Materials Science and Engineering, Cornell University, Ithaca, New York 14853, United States; Department of Chemistry and Chemical Biology, Cornell University, Ithaca, New York 14853, United States

Complete contact information is available at: https://pubs.acs.org/10.1021/acsaelm.3c01329

Author Contributions

**Co-first author: S.X. and M.W. contributed equally. S.X. and M.W. carried out the experiments and analyzed the data. M.B.S. helped carry out experiments for the WTe₂-hBN heterostructures. K.E. conducted the single-crystal XRD experiments. S.X., M.W., N.L.W., and J.J.C. wrote the manuscript with input from all authors. All authors have given approval to the final version of the manuscript.

Notes

The authors declare no competing financial interest.

ACKNOWLEDGMENTS

S.X., M.W., and J.J.C. gratefully acknowledge support from the Gordon and Betty Moore Foundation's EPiQS Initiative, grant GBMF9062.01 and National Science Foundation (CBET #2240944). Device fabrication and characterization for some devices were carried out at the Yale West Campus Materials Characterization Core and the Yale West Campus Cleanroom. This work was performed in part at the Cornell NanoScale Facility, a member of the National Nanotechnology Coordinated Infrastructure (NNCI), which is supported by the National Science Foundation (Grant NNCI-2025233). The authors acknowledge the use of facilities and instrumentation supported by NSF through the Cornell University Materials

Research Science and Engineering Center DMR-1719875. This research used beamline 4-ID of the National Synchrotron Light Source II, a U.S. Department of Energy (DOE) Office of Science User Facility operated for the DOE Office of Science by Brookhaven National Laboratory under Contract No. DE-SC0012704.

REFERENCES

- (1) Zeng, M.; Xiao, Y.; Liu, J.; Yang, K.; Fu, L. Exploring Two-Dimensional Materials toward the Next-Generation Circuits: From Monomer Design to Assembly Control. *Chem. Rev.* **2018**, *118* (13), 6236–6296.
- (2) Voiry, D.; Yamaguchi, H.; Li, J.; Silva, R.; Alves, D. C.; Fujita, T.; Chen, M.; Asefa, T.; Shenoy, V. B.; Eda, G.; Chhowalla, M. Enhanced catalytic activity in strained chemically exfoliated WS₂ nanosheets for hydrogen evolution. *Nat. Mater.* **2013**, *12* (9), 850–5.
- (3) Iannaccone, G.; Bonaccorso, F.; Colombo, L.; Fiori, G. Quantum engineering of transistors based on 2D materials heterostructures. *Nat. Nanotechnol.* **2018**, *13* (3), 183–191.
- (4) Wang, Q. H.; Kalantar-Zadeh, K.; Kis, A.; Coleman, J. N.; Strano, M. S. Electronics and optoelectronics of two-dimensional transition metal dichalcogenides. *Nat. Nanotechnol.* **2012**, *7* (11), 699–712.
- (5) Liu, J.; Cao, H.; Jiang, B.; Xue, Y.; Fu, L. Newborn 2D materials for flexible energy conversion and storage. *Sci. China Mater.* **2016**, *59* (6), 459–474.
- (6) Kim, D.; Pandey, J.; Jeong, J.; Cho, W.; Lee, S.; Cho, S.; Yang, H. Phase Engineering of 2D Materials. *Chem. Rev.* **2023**, 123 (19), 11230–11268.
- (7) Wang, Y.; Xiao, J.; Zhu, H.; Li, Y.; Alsaid, Y.; Fong, K. Y.; Zhou, Y.; Wang, S.; Shi, W.; Wang, Y.; Zettl, A.; Reed, E. J.; Zhang, X. Structural phase transition in monolayer MoTe₂ driven by electrostatic doping. *Nature* **2017**, *550* (7677), 487–491.
- (8) Song, S.; Keum, D. H.; Cho, S.; Perello, D.; Kim, Y.; Lee, Y. H. Room Temperature Semiconductor-Metal Transition of MoTe₂ Thin Films Engineered by Strain. *Nano Lett.* **2016**, *16* (1), 188–93.
- (9) Xiong, F.; Wang, H.; Liu, X.; Sun, J.; Brongersma, M.; Pop, E.; Cui, Y. Li Intercalation in MoS_2 : In Situ Observation of Its Dynamics and Tuning Optical and Electrical Properties. *Nano Lett.* **2015**, *15* (10), 6777–6784.
- (10) Wang, M.; Xu, S.; Cha, J. J. Revisiting Intercalation-Induced Phase Transitions in 2D Group VI Transition Metal Dichalcogenides. *Adv. Energy Sustainability Res.* **2021**, *2* (8), 2100027.
- (11) Keum, D. H.; Cho, S.; Kim, J. H.; Choe, D.-H.; Sung, H.-J.; Kan, M.; Kang, H.; Hwang, J.-Y.; Kim, S. W.; Yang, H.; Chang, K. J.; Lee, Y. H. Bandgap opening in few-layered monoclinic MoTe₂. *Nat. Phys.* **2015**, *11* (6), 482–486.
- (12) Cho, S.; Kim, S.; Kim, J. H.; Zhao, J.; Seok, J.; Keum, D. H.; Baik, J.; Choe, D.-H.; Chang, K. J.; Suenaga, K.; Kim, S. W.; Lee, Y. H.; Yang, H. Phase patterning for ohmic homojunction contact in MoTe₂. Science **2015**, 349 (6248), 625–628.
- (13) Ahmed, S.; Yi, J. Two-Dimensional Transition Metal Dichalcogenides and Their Charge Carrier Mobilities in Field-Effect Transistors. *Nano-Micro Lett.* **2017**, *9* (4), 50.
- (14) Radisavljevic, B.; Radenovic, A.; Brivio, J.; Giacometti, V.; Kis, A. Single-layer MoS₂ transistors. *Nat. Nanotechnol.* **2011**, *6* (3), 147–150.
- (15) Yazdani, S.; Pondick, J. V.; Kumar, A.; Yarali, M.; Woods, J. M.; Hynek, D. J.; Qiu, D. Y.; Cha, J. J. Heterointerface Effects on Lithium-Induced Phase Transitions in Intercalated MoS2. *ACS Appl. Mater. Interfaces* **2021**, *13* (8), 10603–10611.
- (16) Pondick, J. V.; Kumar, A.; Wang, M.; Yazdani, S.; Woods, J. M.; Qiu, D. Y.; Cha, J. J. Heterointerface Control over Lithium-Induced Phase Transitions in MoS₂ Nanosheets: Implications for Nanoscaled Energy Materials. *ACS Appl. Nano Mater.* **2021**, 4 (12), 14105–14114.

- (17) Pondick, J. V.; Yazdani, S.; Kumar, A.; Hynek, D. J.; Hart, J. L.; Wang, M.; Qiu, D. Y.; Cha, J. J. Thickness-dependent phase transition kinetics in lithium-intercalated MoS₂. 2D Mater. **2022**, 9 (2), 025009.
- (18) Lappalainen, J.; Kangaspuoskari, M. Interface Effects of Strain-Energy Potentials on Phase Transition Characteristics of VO₂ Thin-Films. ACS Omega 2023, 8 (23), 21083–21095.
- (19) Fei, Z.; Palomaki, T.; Wu, S.; Zhao, W.; Cai, X.; Sun, B.; Nguyen, P.; Finney, J.; Xu, X.; Cobden, D. H. Edge conduction in monolayer WTe₂. *Nat. Phys.* **2017**, *13* (7), 677–682.
- (20) Fatemi, V.; Wu, S.; Cao, Y.; Bretheau, L.; Gibson, Q. D.; Watanabe, K.; Taniguchi, T.; Cava, R. J.; Jarillo-Herrero, P. Electrically tunable low-density superconductivity in a monolayer topological insulator. *Science* **2018**, 362 (6417), 926–929.
- (21) Sajadi, E.; Palomaki, T.; Fei, Z.; Zhao, W.; Bement, P.; Olsen, C.; Luescher, S.; Xu, X.; Folk, J. A.; Cobden, D. H. Gate-induced superconductivity in a monolayer topological insulator. *Science* **2018**, 362 (6417), 922–925.
- (22) Zhu, L.; Li, Q. Y.; Lv, Y. Y.; Li, S.; Zhu, X. Y.; Jia, Z. Y.; Chen, Y. B.; Wen, J.; Li, S. C. Superconductivity in Potassium-Intercalated T_d-WTe₂. *Nano Lett.* **2018**, *18* (10), 6585–6590.
- (23) Fei, Z.; Zhao, W.; Palomaki, T. A.; Sun, B.; Miller, M. K.; Zhao, Z.; Yan, J.; Xu, X.; Cobden, D. H. Ferroelectric switching of a two-dimensional metal. *Nature* **2018**, *560* (7718), 336–339.
- (24) Muscher, P. K.; Rehn, D. A.; Sood, A.; Lim, K.; Luo, D.; Shen, X.; Zajac, M.; Lu, F.; Mehta, A.; Li, Y.; Wang, X.; Reed, E. J.; Chueh, W. C.; Lindenberg, A. M. Highly Efficient Uniaxial In-Plane Stretching of a 2D Material via Ion Insertion. *Adv. Mater.* **2021**, 33 (37), 2101875.
- (25) Wang, M.; Kumar, A.; Dong, H.; Woods, J. M.; Pondick, J. V.; Xu, S.; Hynek, D. J.; Guo, P.; Qiu, D. Y.; Cha, J. J. A Gapped Phase in Semimetallic Td-WTe₂ Induced by Lithium Intercalation. *Adv. Mater.* **2022**, *34* (24), 2200861.
- (26) Zhou, Y.; Silva, J. L.; Woods, J. M.; Pondick, J. V.; Feng, Q.; Liang, Z.; Liu, W.; Lin, L.; Deng, B.; Brena, B.; Xia, F.; Peng, H.; Liu, Z.; Wang, H.; Araujo, C. M.; Cha, J. J. Revealing the Contribution of Individual Factors to Hydrogen Evolution Reaction Catalytic Activity. *Adv. Mater.* **2018**, *30* (18), 1706076.
- (27) Ma, X.; Guo, P.; Yi, C.; Yu, Q.; Zhang, A.; Ji, J.; Tian, Y.; Jin, F.; Wang, Y.; Liu, K.; Xia, T.; Shi, Y.; Zhang, Q. Raman scattering in the transition-metal dichalcogenides of 1T'-MoTe₂, Td-MoTe₂, and Td-WTe₂. Phys. Rev. B **2016**, 94 (21), 214105.
- (28) Nair, J. R.; Gerbaldi, C.; Destro, M.; Bongiovanni, R.; Penazzi, N. Methacrylic-based solid polymer electrolyte membranes for lithium-based batteries by a rapid UV-curing process. *React. Funct. Polym.* **2011**, *71* (4), 409–416.
- (29) Whittingham, M. S.; Gamble, F. R., Jr. The lithium intercalates of the transition metal dichalcogenides. *Mater. Res. Bull.* **1975**, *10* (5), 363–371.
- (30) Xiang, F.-X.; Srinivasan, A.; Du, Z. Z.; Klochan, O.; Dou, S.-X.; Hamilton, A. R.; Wang, X.-L. Thickness-dependent electronic structure in WTe₂ thin films. *Phys. Rev. B* **2018**, *98* (3), 035115.
- (31) Lee, C.-H.; Ryu, H.; Nolan, G.; Zhang, Y.; Lee, Y.; Oh, S.; Cheong, H.; Watanabe, K.; Taniguchi, T.; Kim, K.; Lee, G.-H.; Huang, P. Y. In Situ Imaging of an Anisotropic Layer-by-Layer Phase Transition in Few-Layer MoTe₂. *Nano Lett.* **2023**, 23 (2), 677–684.
- (32) Parida, S.; Mishra, A.; Chen, J.; Wang, J.; Dobley, A.; Carter, C. B.; Dongare, A. M. Vertically Stacked 2H-1T Dual-Phase MoS₂ Microstructures during Lithium Intercalation: A First Principles Study. *J. Am. Ceram. Soc.* **2020**, *103* (11), 6603–6614.
- (33) Sung, S. H.; Schnitzer, N.; Novakov, S.; El Baggari, I.; Luo, X.; Gim, J.; Vu, N. M.; Li, Z.; Brintlinger, T. H.; Liu, Y.; Lu, W.; Sun, Y.; Deotare, P. B.; Sun, K.; Zhao, L.; Kourkoutis, L. F.; Heron, J. T.; Hovden, R. Two-dimensional charge order stabilized in clean polytype heterostructures. *Nat. Commun.* **2022**, *13* (1), 413.
- (34) Pondick, J. V.; Yazdani, S.; Yarali, M.; Reed, S. N.; Hynek, D. J.; Cha, J. J. The Effect of Mechanical Strain on Lithium Staging in Graphene. *Adv. Electron. Mater.* **2021**, *7* (3), 2000981.
- (35) Yang, W.; Yuan, Z.-Y.; Luo, Y.-Q.; Yang, Y.; Zheng, F.-W.; Hu, Z.-H.; Wang, X.-H.; Liu, Y.-A.; Zhang, P. Raman-active modes of 1T'

- WTe₂ under tensile strain: A first-principles prediction. *Phys. Rev.* B **2019**, 99 (23), 235401.
- (36) Yang, W.; Fu, S.-B.; Lu, Y.; Zhang, K.-Y.; Liu, J.-M.; Gao, H.-R.; Wang, X.-H.; Liu, Y.-A.; Zhang, P. Response of Raman-active modes in monolayer 1T'-WTe $_2$ to charge doping. *Phys. Rev. B* **2022**, *106* (20), 205415.
- (37) Hong, S. S.; Kundhikanjana, W.; Cha, J. J.; Lai, K.; Kong, D.; Meister, S.; Kelly, M. A.; Shen, Z.-X.; Cui, Y. Ultrathin Topological Insulator Bi2Se3 Nanoribbons Exfoliated by Atomic Force Microscopy. *Nano Lett.* **2010**, *10* (8), 3118–3122.
- (38) Cadore, A. R.; Mania, E.; Alencar, A. B.; Rezende, N. P.; de Oliveira, S.; Watanabe, K.; Taniguchi, T.; Chacham, H.; Campos, L. C.; Lacerda, R. G. Enhancing the response of NH3 graphene-sensors by using devices with different graphene-substrate distances. *Sens. Actuators, B* **2018**, *266*, 438–446.
- (39) Xu, H.; Wu, J.; Chen, Y.; Zhang, H.; Zhang, J. Substrate Engineering by Hexagonal Boron Nitride/SiO2 for Hysteresis-Free Graphene FETs and Large-Scale Graphene p—n Junctions. *Chem. Asian J.* **2013**, *8* (10), 2446–2452.
- (40) Pantano, M. F.; Iacob, E.; Picciotto, A.; Margesin, B.; Centeno, A.; Zurutuza, A.; Galiotis, C.; Pugno, N. M.; Speranza, G. Investigation of charges-driven interactions between graphene and different SiO₂ surfaces. *Carbon* **2019**, *148*, 336–343.